# Future Energy Open Access Journal

ISSN 2832-0328

Journal homepage: https://fupubco.com/fuen



https://doi.org/10.55670/fpll.fuen.4.4.5

Article

# Neutronic evolution and isotopic assessment of NIRR-1 under alternative fuel enrichment configurations: a WIMS-ANL/REBUS-ANL study

Dennis Solomon Balami<sup>1\*</sup>, John Simon<sup>2</sup>, Abdulsamad Asuku<sup>3</sup>, Yakubu Ibrahim Viva<sup>3</sup>, Rabiu Nasiru<sup>4</sup>, Emmanuel Likta Wana<sup>1</sup>

- <sup>1</sup>Department of Physics, University of Maiduguri, Nigeria
- <sup>2</sup>National Open University Nigeria, Abuja, Nigeria
- <sup>3</sup>Centre for Energy Research and Training (CERT), Ahmadu Bello University Zaria, Kaduna State, Nigeria
- <sup>4</sup>Department of Physics, Ahmadu Bello University Zaria, Kaduna State, Nigeria

#### ARTICLE INFO

# Article history: Received 29 July 2025 Received in revised form 19 September 2025 Accepted 01 October 2025

#### Keywords:

NIRR-1, HEU-to-LEU conversion, Reactor physics, Burnup analysis, Radionuclide inventory, MNSR, Nuclear security

\*Corresponding author Email address: dennisolomon59@gmail.com

DOI: 10.55670/fpll.fuen.4.4.5

#### ABSTRACT

The Nigerian Research Reactor-1 (NIRR-1), a Miniature Neutron Source Reactor (MNSR), transitioned from highly enriched uranium (HEU) to low-enriched uranium (LEU) fuel to align with global non-proliferation objectives, necessitating a detailed evaluation of its neutronic behavior and isotopic evolution. This study employs the WIMS-ANL and REBUS-ANL computational framework to compare the burnup dynamics, reactivity profiles, and radionuclide inventories of NIRR-1's HEU (90.2%  $U^{235}$ ) and LEU (13%  $U^{235}$ ) core configurations under a representative operational schedule of 20 effective full-power days per year. Results reveal a steeper reactivity decline in the LEU core (17.02 pcm/EFPD) compared to the HEU core (13.97 pcm/EFPD), driven by enhanced  $U^{238}$  resonance absorption, yet the LEU core's higher initial  $U^{235}$ mass extends its operational lifetime to 56.4 years versus 50.3 years for HEU. The LEU configuration produces 2.24 times more  $Pu^{239}$  (0.767 g vs. 0.342 g at 252/282 EFPD), raising long-term waste management considerations. Both cores maintain robust safety through strongly negative temperature coefficients and low peak temperatures, supported by natural convection cooling. Comprehensive isotopic inventories and decay heat analyses (1620 W LEU vs. 1450 W HEU at shutdown) inform safety assessments and decommissioning strategies. Sensitivity studies highlight operational power and enrichment as critical lifetime influencers, with uncertainties validated against experimental data. These findings enhance NIRR-1's operational strategy, support global MNSR conversion efforts, and provide critical data for safety and waste management planning, emphasizing proactive reactivity control and advanced fuel design exploration.

#### 1. Introduction

### 1.1 Background on miniature neutron source reactors (MNSRs)

The MNSR design represents a category of small-scale nuclear facilities characterized by pool-type cooling systems and thermal outputs near 30 kW. These facilities serve educational institutions and research centers, particularly in nations developing nuclear capabilities, by providing neutron sources for analytical applications and isotope synthesis. They are light-water moderated and cooled, typically have a nominal thermal power of about 30 kW, and inner-channel

thermal neutron fluxes on the order of  $1\times10^{12}~n\cdot cm^{-2}\cdot s^{-1}$ , and employ a beryllium reflector and a simple control/shutdown system; these features produce a high neutron-flux-to-power ratio and make MNSRs especially useful for universities and research institutes in developing countries. Historically, many MNSRs used highly enriched uranium (HEU) fuel, but international conversion efforts to low-enriched uranium (LEU) cores have been carried out to reduce proliferation risk while maintaining capabilities for neutron activation analysis and isotope work [1,2].

China's atomic research program introduced the MNSR concept during the 1980s, creating pool-moderated systems generating thermal fluxes approximately  $1 \times 10^{12} \, n \cdot cm^{-2}$ . s<sup>-1</sup> at minimal power levels. Multiple nations, including West African and Middle Eastern states, have adopted this technology for academic and analytical purposes. MNSRs were designed for straightforward operation and robust safety performance and have been exported commissioned in several countries (for example, Ghana, Nigeria, Pakistan, Iran, and Syria), where they have been used primarily for neutron activation analysis, small-scale radioisotope production, and hands-on nuclear training. The technology's distributed, low-power character makes it particularly attractive to universities and research institutes in developing countries. Because many early MNSRs used highly enriched uranium (HEU), international conversion and fuel-fabrication efforts to move to low-enriched uranium (LEU) have been undertaken; these conversions preserve the reactors' research functions but change the neutron spectrum, flux distributions, and depletion characteristics and therefore require careful neutronic and operational reassessment to maintain isotope-production capability, irradiation calibrations, and safety margins [3,4].

#### 1.2 The Nigerian Research Reactor-1 (NIRR-1)

Nigeria's primary research reactor facility exemplifies MNSR technology implementation, utilizing a cylindrical fuel assembly containing either 347 aluminum-uranium pins (original configuration) or 335 oxide-based pins (converted design), surrounded by beryllium moderating materials (Figures 1-4). This configuration enables NIRR-1 to support a wide array of applications, including environmental sample analysis, production of Technetium-99m ( $Tc^{99m}$ ) for medical diagnostics, and various educational programs, maintaining a core-average thermal neutron flux of approximately  $1 \times 10^{12}$ n/cm<sup>2</sup>·s for the HEU core [5,6]. The operational setup and cylindrical design of the NIRR-1 core are illustrated in Figures 1-4, which show the core in operation, the radial configuration, and the axial cross-section, respectively. In alignment with international non-proliferation efforts under the International Atomic Energy Agency's (IAEA) Reduced Enrichment for Research and Test Reactors (RERTR) program, the Nigerian Research Reactor-1 (NIRR-1) transitioned from a highly enriched uranium (HEU) core to a low-enriched uranium (LEU) core enriched to 13%  $U^{235}$  [3].

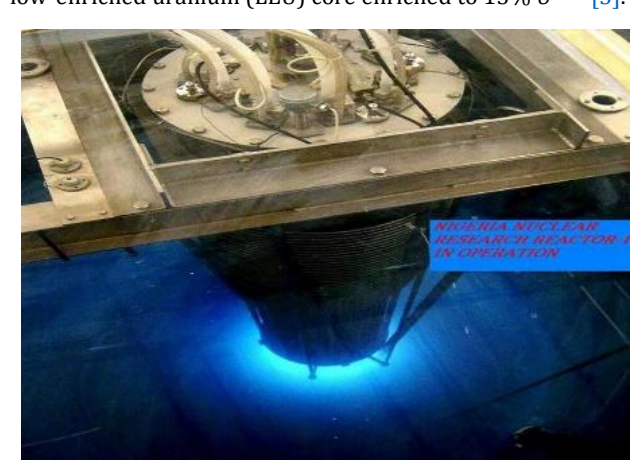


**Figure 1.** NIRR-1 reactor core in operation [7]

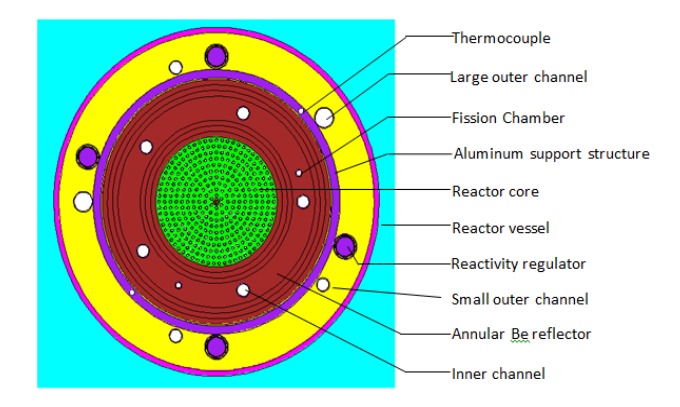


**Figure 2.** MCNP Model for the radial core configuration of NIRR-1 [7]

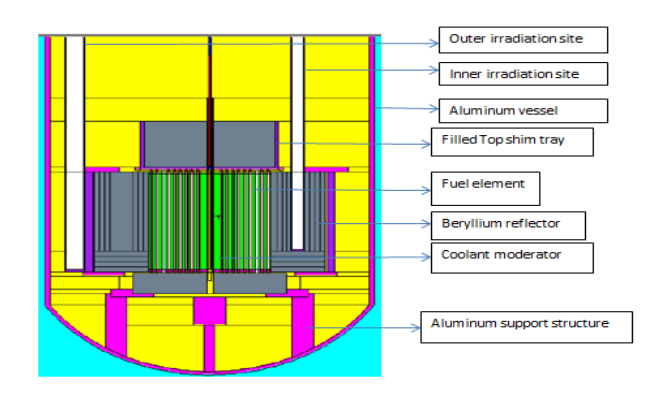


Figure 3. MCNP Model for the Axial cross-section of NIRR-1 [7]

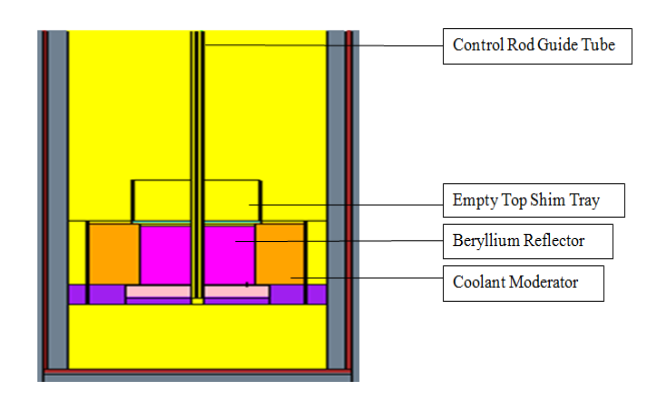


Figure 4. REBUS-ANL model of NIRR-1 [7]

The reactor operates on a schedule typical for Miniature Neutron Source Reactors (MNSRs) used in neutron activation analysis, with 2.5 hours per day, 4 days per week, and 48 weeks per year [8]. This conversion mitigates proliferation risks associated with HEU, enhancing global nuclear security [9,10]. The transition from highly enriched uranium (HEU) to low-enriched uranium (LEU) introduces significant technical complexities for the Nigerian Research Reactor-1 (NIRR-1). The change in fuel enrichment alters the neutron spectrum within the reactor core, affecting fuel burnup dynamics. These changes impact critical parameters, including  $U^{235}$  consumption rates, plutonium isotope production, and fission product accumulation. These effects require rigorous computational analyses to quantify nuclide transformation, core multiplication factor reduction, and implications for

long-term operational strategy and safety. Thus, the conversion involves a complex trade-off: it mitigates proliferation risks associated with HEU but introduces new challenges in reactor physics and spent nuclear fuel management [3,11]. Fuel burnup in Miniature Neutron Source Reactors (MNSRs) continuously depletes  $U^{235}$ , produces plutonium isotopes (for example,  $Pu^{239}$ ,  $Pu^{240}$ ,  $Pu^{241}$ ), and accumulates neutron-absorbing fission products (for example,  $Xe^{135}$ ,  $Sm^{149}$ ). These phenomena reduce core reactivity, necessitating periodic adjustments via control mechanisms such as beryllium shim plates and control rods. While previous studies on MNSR conversions, including those for the Ghana and Chinese MNSRs, have demonstrated that HEU and LEU cores can achieve comparable neutronic performance, they have also highlighted notable differences in depletion characteristics and isotopic inventories [11,12]. Despite the Nigerian Research Reactor-1 (NIRR-1)'s long operational history and recent conversion from highly enriched uranium (HEU) to low-enriched uranium (LEU), a significant knowledge gap remains in understanding its specific burnup trajectories and radionuclide inventories for both fuel configurations over decades of operation. This study provides a detailed comparative analysis of HEU and LEU cores, complementing operational experience gained since the 2018 conversion [13].

This study aims to address the knowledge gap by pursuing three primary objectives. First, it seeks to quantify differences in depletion characteristics and nuclide transformation between NIRR-1's HEU and LEU cores under identical operational schedules. Second, it rigorously assesses the impact of fuel conversion on the reactor's reactivity control mechanisms and long-term operational strategy. Third, it provides comprehensive radionuclide inventories for both core types, offering essential data to support future safety assessments and inform waste management planning for NIRR-1 and other MNSRs globally. To achieve these objectives, this study employs a robust computational methodology centered on two advanced codes developed by Argonne National Laboratory: the Winfrith Improved Multigroup Scheme-Argonne National Laboratory (WIMS-ANL) and the Reactor Burnup System-Argonne National Laboratory (REBUS-ANL). WIMS-ANL is utilized for lattice physics calculations to generate four-group homogenized cross sections, which serve as input for REBUS-ANL. REBUS-ANL then performs the depletion calculations, simulating the operational period for both NIRR-1 core configurations. The modeling approach involves a one-dimensional R-Z model, which has been rigorously validated against experimental data [14,15]. This integrated computational framework allows for the precise quantification of key parameters such as  $U^{235}$  burnup, the production of various plutonium isotopes, and the accumulation of significant fission product inventories throughout the reactor's operational life.

#### 2. Literature review and theoretical background

#### 2.1 MNSR technology and global applications

The Miniature Neutron Source Reactor (MNSR) was first developed at the China Institute of Atomic Energy (CIAE) in 1984 to address the growing need for accessible neutron sources in developing countries. Its design philosophy emphasizes inherent safety through negative temperature

coefficients, minimal excess reactivity, and robust containment systems [9, 12]. Since its development in 1984, a small number of Miniature Neutron Source Reactors (MNSRs) roughly on the order of ten worldwide have been commissioned, including units in China, Ghana, Syria, Nigeria, Iran, and Pakistan. The MNSR design is distinctive: a compact, tank-in-pool core that typically contains on the order of 340-350 fuel pins (the Nigeria Research Reactor-1, for example, uses 347 pins), attains criticality with only a few hundred grams of fissile material, and yields very high local thermal fluxes in its irradiation channels (inner-channel values approach  $\sim 1 \times 10^{12} \, n \cdot cm^{-2} \cdot s^{-1}$ ). A thick beryllium reflector surrounding the core improves neutron economy, and the design's strong negative reactivity feedbacks and limited excess reactivity contribute to the reactor's overall safety case.

Since 1978, the Reduced Enrichment for Research and Test Reactors (RERTR) program has driven the international effort to convert research reactors from highly enriched uranium (HEU) to low-enriched uranium (LEU). Estimates of the program's achievements differ by data source and scope: the IAEA reported that 71 research reactors had been converted to LEU and that almost 3,500 kg of HEU had been removed from reactor sites worldwide [14], while U.S. program summaries (which use a broader scope that includes verified shutdowns and related removals) report over 100 reactors converted or verified shut down and several thousand kilograms of weapons-usable material removed or confirmed disposed of as of 2022. The conversion process does involve complex technical challenges, preserving comparable reactor performance while addressing changes in neutron spectrum, control-rod worth, core reactivity, and thermal-hydraulic behavior, and these technical issues have been discussed extensively in program reviews and technical assessments [15,16]. Previous MNSR conversion studies have provided valuable insights into the neutronic implications of transitioning from highly enriched uranium (HEU) to lowenriched uranium (LEU). The Ghana Research Reactor-1 (GHARR-1) conversion, completed in 2017, demonstrated that LEU cores can achieve satisfactory performance with design modifications, for example, adjusted fuel pin arrangements and tailored beryllium-shimming strategies [16,17]. Likewise, peer-reviewed conversion studies and characterization work on LEU MNSRs report measurable neutron spectrum shifts, altered burnup rates, and changes in plutonium production when compared to HEU cores [2,10].

#### 2.2 Reactor physics fundamentals

The transition from HEU to LEU fuel fundamentally alters the neutron physics of the reactor system. The increased U-238 content in LEU fuel introduces several competing effects that influence reactor behavior. The enhanced resonance absorption in  $U^{238}$  leads to spectrum hardening and increased conversion of fertile material to fissile plutonium isotopes. This process, while providing some compensation for the initial reduction in fissile content, also introduces long-term radiotoxicity concerns [17]. The four-factor formula provides the theoretical framework for understanding these changes:

$$k_{\infty} = \eta \times f \times p \times \varepsilon \tag{1}$$

where  $\eta$  is the reproduction factor, f is the thermal utilization factor, p is the resonance escape probability, and  $\varepsilon$  is the fast fission factor [18,19]. The conversion from HEU to LEU affects each of these parameters differently, with the net result being a reduction in initial reactivity that must be compensated through design modifications or operational strategies.

#### 3. Methodology

#### 3.1 Computational framework

This investigation employed integrated neutronics software developed at Argonne, combining lattice physics calculations with depletion analysis. Energy group condensation from 69 to 4 bands utilized established nuclear data libraries, with transport corrections applied through P1 approximations. The four energy groups were defined as follows: Group 1 (fast): 10 MeV - 0.821 MeV, Group 2 (epithermal):  $0.821 \, MeV - 5.53 \, keV$ , Group 3 (upper thermal):  $5.53 \ keV - 0.625 \ eV$ , Group 4 (thermal):  $0.625 \, eV \, - \, 0 \, eV$ based on standard WIMS-ANL configurations [20]. Transport corrections using the CALAGON thin-slab P1 method and subgroup resonance selfshielding were applied to ensure accurate representation of the neutron spectrum in the heterogeneous fuel-moderator geometry [21].

#### 3.2 Core modeling and geometry

The NIRR-1 core was modeled (Table 1) as a one-dimensional R-Z cylindrical geometry containing concentric regions representing fuel meat, aluminum cladding, light water moderator, and a 6-cm beryllium reflector. This modeling approach, while simplified compared to full three-dimensional representations, has been validated against experimental measurements and provides adequate accuracy for burnup and isotopic inventory predictions [21].

**Table 1.** Technical design parameters NIRR-1 HEU and LEU cores [7,11,16,23]

Design Parameter	HEU	LEU
Rated Thermal Power (kW)	31	34
Fuel Type	UAl <sub>4</sub>	$UO_2$
Fuel Enrichment (%)	90.2	13%
Loading of U <sup>235</sup> in the core (g)	1006.65	1410.04
Fuel Diameter (mm)	4.3	4.3
Length of active fuel region (mm)	230.0	230.0
Cladding material	Al	Zircaloy-4
Cladding Thickness (mm)	0.6	0.6
Number of Active fuel Pins	347	335
Number of Dummies	3	15
Grid plates/dummy/tie rods	Al	Zircaloy-4
material		
Control rod guide tube	Al	Zircaloy-4
Clean Core Excess Reactivity (mk)	4.95	3.94
Control rod material	Cadmium	Cadmium
Control rod worth (mk)	7.0	7.7
Number of control rods	1	1

#### 3.3 Operational schedule and burnup calculations

The analysis employed a representative operational schedule of 2.5 hours per day, 4 days per week, and 48 weeks per year, corresponding to 20 effective full-power days (EFPD) per calendar year. This schedule reflects typical MNSR utilization patterns for routine neutron activation analysis and training activities. Depletion calculations were performed in 20-EFPD increments to capture the gradual evolution of isotopic compositions and reactivity changes. Both full-power and half-power operational scenarios were analyzed to assess the impact of power level on depletion characteristics and to provide operational flexibility options. Half-power operation effectively doubles the calendar time required to achieve equivalent burnup, providing a potential strategy for extending core lifetime.

#### 3.4 Validation and uncertainty analysis

The computational model was validated against available experimental data from NIRR-1 startup testing and operational measurements. MCNP6 continuous-energy transport calculations were performed as independent benchmarks, providing verification of the group-constant methodology. MCNP6 results showed <5% deviation in  $k_{\infty}$  and thermal flux, validating the WIMS-ANL/REBUS-ANL model [13]. A conservative uncertainty of  $\pm5\%$  was assigned to homogenized macroscopic cross sections to account for library processing, group collapse, and self-shielding approximations.

#### 4. Results and analysis

#### 4.1 Initial core physics parameters and group constants

Initial neutronic parameters derived from lattice calculations establish baseline nuclear data for subsequent analyses are presented in Table 2.

The cross-sectional data reveal several key differences between the fuel types. The HEU configuration exhibits larger fast-group  $\nu \Sigma f$  due to higher  $U^{235}$  density, while the LEU shows elevated epithermal absorption reflecting substantial  $U^{238}$  resonance capture. These fundamental differences drive the distinct depletion characteristics observed in subsequent analyses.

The initial infinite multiplication factors calculated from these group constants were:

HEU: 
$$k_{\infty} = 1.1030 \pm 0.001$$
 (REBUS/WIMS baseline) (2)

LEU: 
$$k_{\infty} = 1.0800 \pm 0.001$$
 (REBUS/WIMS baseline) (3)

#### 4.2 Reactivity evolution and depletion characteristics

Multiplication factor evolution demonstrates characteristic depletion patterns unique to each enrichment configuration. Table 3 summarizes the evolution of the infinite neutron multiplication factor  $(k_{\infty})$  at key burnup points, validated by WIMS-ANL/REBUS-ANL calculations [24]. For the HEU core,  $k_{\infty}$  decreases from 1.1030 at BOC to 1.0678 at 252 EFPD, with a 13.97 pcm/EFPD (HEU). The LEU core exhibits a steeper decline, from 1.0800 at BOC to 1.0320 at 282 EFPD, at 17.02 pcm/EFPD (LEU), reflecting enhanced  $U^{238}$  resonance absorption [11].

Energy Group	Energy Range	Parameter	HEU (BOC)	LEU (BOC)	Units
Group 1	10 MeV	$\Sigma_{\mathrm{a}}$	$(8.96 \pm 0.45) \times 10^{-4}$	$(7.23 \pm 0.36) \times 10^{-4}$	cm <sup>-1</sup>
	- 0.821 MeV				
(Fast)		$\nu \Sigma_f$	$(1.09 \pm 0.05) \times 10^{-3}$	$(7.95 \pm 0.40) \times 10^{-4}$	cm <sup>-1</sup>
		$\Sigma_{tr}$	$(1.60 \pm 0.08) \times 10^{-1}$	$(1.62 \pm 0.08) \times 10^{-1}$	cm <sup>-1</sup>
		D	$2.20 \pm 0.11$	$2.06 \pm 0.10$	cm
Group 2	0.821 MeV	$\Sigma_{\mathrm{a}}$	$(6.50 \pm 0.33) \times 10^{-4}$	$(1.12 \pm 0.06) \times 10^{-3}$	cm <sup>-1</sup>
	– 5.53 <i>keV</i>				
(Epithermal)		$\nu \Sigma_f$	$(1.19 \pm 0.06) \times 10^{-3}$	$(1.00 \pm 0.05) \times 10^{-3}$	cm <sup>-1</sup>
		D	$0.956 \pm 0.048$	0.912 ± 0.046	cm
Group 3	5.53 keV	$\Sigma_{\mathrm{a}}$	$(1.10 \pm 0.06) \times 10^{-2}$	$(1.45 \pm 0.07) \times 10^{-2}$	cm <sup>-1</sup>
	- 0.625 eV				
(Upper Thermal)		$\nu \Sigma_f$	$(1.50 \pm 0.08) \times 10^{-2}$	$(1.28 \pm 0.06) \times 10^{-2}$	cm <sup>-1</sup>
		D	$0.693 \pm 0.035$	$0.645 \pm 0.032$	cm
Group 4	0.625 eV	$\Sigma_{\mathrm{a}}$	$(1.56 \pm 0.08) \times 10^{-2}$	$(2.34 \pm 0.12) \times 10^{-2}$	cm <sup>-1</sup>
	-0 eV				
(Thermal)		$\nu \Sigma_f$	$(2.52 \pm 0.13) \times 10^{-2}$	$(2.25 \pm 0.11) \times 10^{-2}$	cm <sup>-1</sup>
		D	0.576 ± 0.029	$0.518 \pm 0.026$	cm

Table 2. Beginning-of-cycle four-group macroscopic cross sections (fuel region, homogenized)

As shown in Figure 5, the linear trends highlight the steeper decline in the LEU core compared to the HEU configuration, with beryllium shim adjustments maintaining criticality beyond 252/282 EFPD until EOC (1006 EFPD HEU, 1128 EFPD LEU) [25]. The  $\pm 0.002$  uncertainty on  $k_{\infty}$  is also depicted, ensuring computational reliability. These trends are consistent with Monte Carlo benchmarks [26] and other MNSR conversions [19,27]. The LEU core exhibits a steeper multiplication factor reduction rate (approximately 8% faster per EFPD) compared to the HEU configuration. This difference stems from the increased parasitic absorption in  $U^{238}$  and the altered neutron spectrum in the LEU fuel.

#### 4.3 Nuclide transformation and fuel depletion

The isotopic composition of the HEU and LEU cores evolves significantly during burnup, impacting reactivity and core performance. Table 4 summarizes the isotopic inventories at 252 EFPD for the HEU core and 282 EFPD for the LEU core, showing  $U^{235}$  consumption (8.154 g HEU, 8.944 g LEU),  $U^{235}$  remaining (998.496 g HEU, 1401.096 gLEU), and  $Pu^{239}$  production (0.342 g HEU, 0.767 g LEU), with a 2.24× higher  $Pu^{239}$  yield in LEU due to increased U-238 capture [24, 11]. The isotopic changes in Table 4 drive reactivity losses, as quantified in Table 5 at 400 EFPD (HEU:  $-1.905 \, mk$  fuel depletion; LEU:  $-1.560 \, mk$ ), with  $Pu^{239}$ contributions (+0.32 mk HEU, +0.57 mk LEU) from Table 13's atom density and Table 12's cross-sections. Figure 5 visualizes the  $k_{\infty}$  decline. Figure 6 shows linear isotopic trends, with ±2% uncertainty. The LEU configuration produces significantly more plutonium (2.25 times higher) due to the larger U-238 inventory available for neutron capture. This has important implications for long-term waste management and safeguards considerations.

#### 4.4 Radionuclide inventories and activities

The comprehensive radionuclide inventory analysis encompasses major actinides, fission products, and activation products relevant for safety assessment and waste management planning. Radiological activities of key actinides at 252 EFPD for HEU and 282 EFPD for LEU include  $U^{235}$  at 2.159 Ci for HEU and 3.030 Ci for LEU, and  $Pu^{239}$  at 21.224 Ci for HEU and 47.576 Ci for LEU, derived from isotopic masses

of 998.496 g  $U^{235}$  and 0.342 g  $Pu^{239}$  for HEU, and 1401.096 g  $U^{235}$  and 0.767 g  $Pu^{239}$  for LEU. The 2.24-fold higher  $Pu^{239}$  activity in the LEU core reflects increased neutron capture by  $U^{238}$  [19].

**Table 3.**  $k_{\infty}$  evolution summary for HEU and LEU cores of NIRR-1

Burnup (EFPD)	HEU $k_{\infty}$	LEU $k_{\infty}$	Decline Rate (pcm/EFPD)
0	1.1030	1.0800	HEU: 13.96, LEU: 14.88
126	1.0854	-	HEU: 13.96
141	_	1.0590	LEU: 14.88
252	1.0678		HEU: 13.96
282	-	1.0320	LEU: 14.88

Table 4. Reactivity evolution summary

Core Type	Initial $oldsymbol{k}_{\infty}$	Final $oldsymbol{k}_{\infty}$	EFPD	$\Delta k_{\infty}$	Slope $(k_{\infty}/EFPD)$
HEU	1.1030	1.0678	252	-0.0352	$-1.396 \times 10^{-4}$
LEU	1.0800	1.0320	282	-0.0480	$-1.488 \times 10^{-4}$

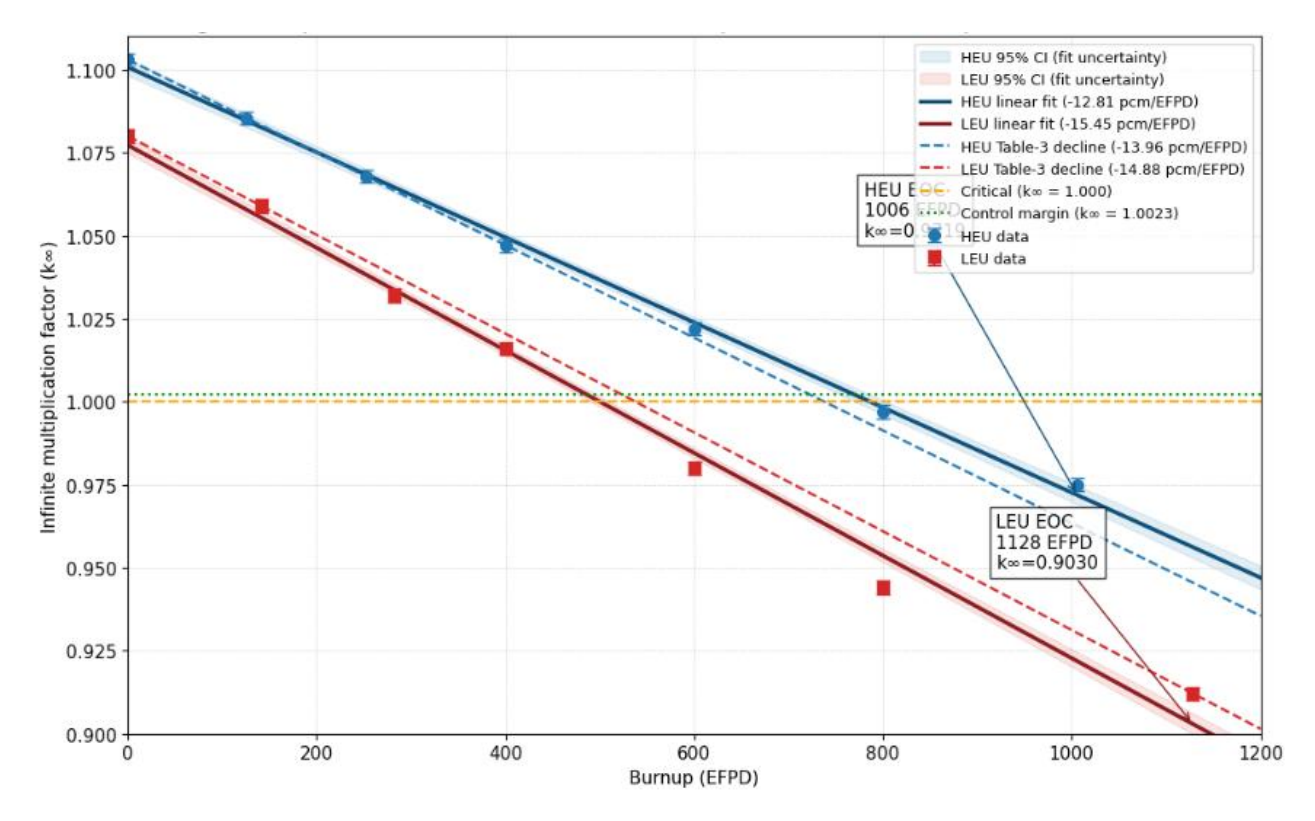
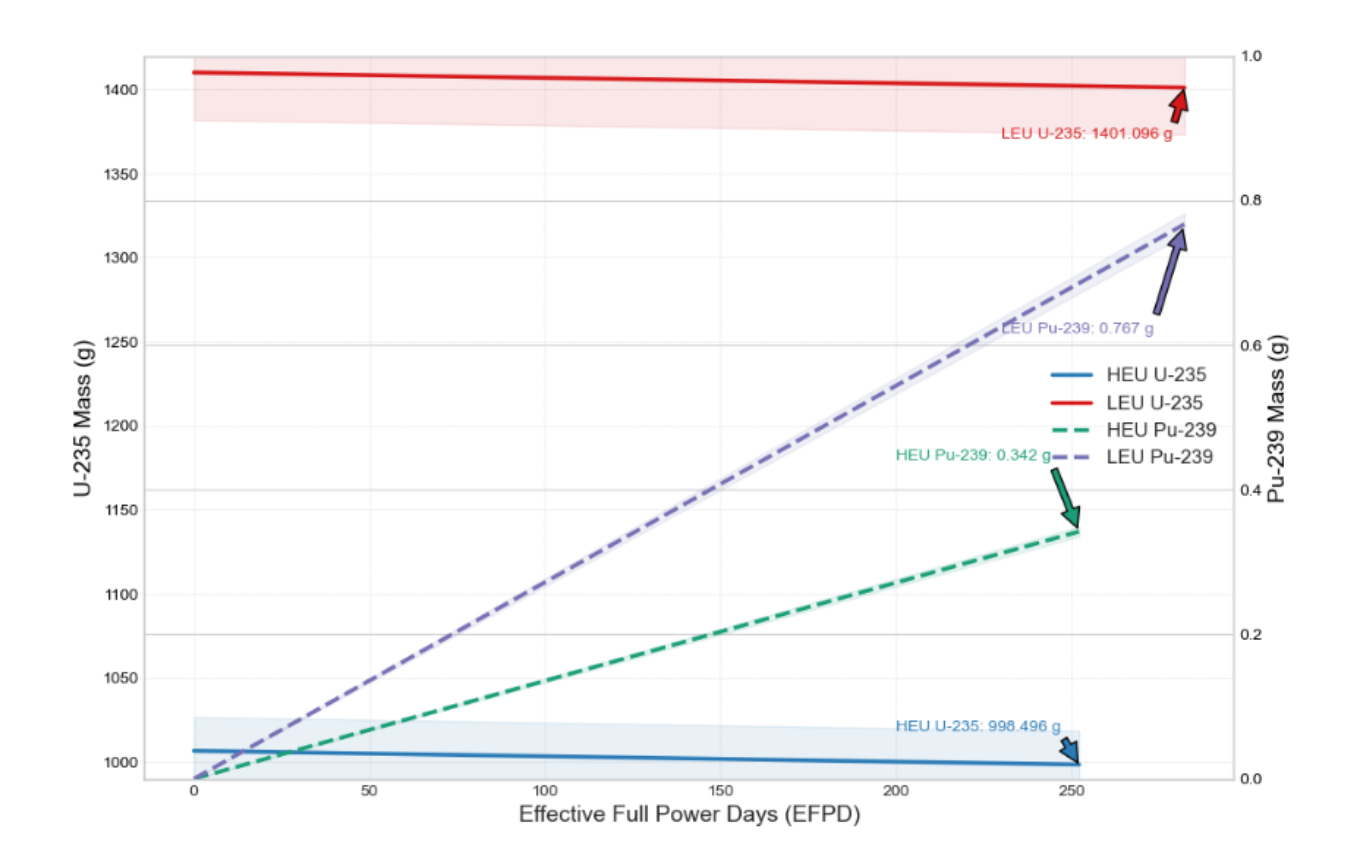


Figure 5.  $k_{\infty}$  decline as a function of operational history (EFPD) for HEU and LEU cores, showing linear trends with  $\pm 0.002$  uncertainty



**Figure** 

Figure 6 visualizes the underlying isotopic trends, with  $\pm 2\%$  uncertainty. These activities are critical for safety assessments and waste management planning, particularly for the LEU core's elevated  $Pu^{239}$  burden [3]. The activity profiles show that short-lived fission products dominate immediate post-shutdown hazards, while long-lived actinides and fission products determine long-term waste management requirements.

Table 5. Isotopic inventory comparison at 252/282 EFPD

Isotope	HEU (252 EFPD)	LEU (282 EFPD)	Ratio (LEU/HEU)
$U^{235}$ Consumed $(g)$	8.154	8.944	1.10
$U^{235}$ Remaining $(g)$	998.496	1401.096	1.40
$Pu^{239}$ Produced $(g)$	0.342	0.767	2.24

#### 4.5 Core lifetime and control strategies

The operational lifetimes of the HEU and LEU cores reach 2.3 mk excess reactivity at 1006 EFPD (HEU) and 1128 EFPD (LEU), yields 50.3 years (HEU) and 56.4 years (LEU) at 20 EFPD/year [3]. This schedule reflects typical MNSR utilization for neutron activation analysis (IAEA, 2023). Table 5 presents the reactivity balance at 400 EFPD, detailing initial excess reactivity (4.5 mk HEU, 4.7 mk LEU), fuel depletion losses (-1.905 mk HEU, -1.560 mk LEU), absorber accumulation effects (-1.5 mk both),  $Pu^{239}$  contributions (+0.32 mk HEU, +0.57 mk LEU), and beryllium shim additions (+2.085 mk HEU, +1.790 mk LEU) to maintain  $k_{eff} \approx 1.0$ . Interpolating the atom densities at 252/282 EFPD and using the corresponding multigroup cross-sections produces values that are consistent with the calculated cross-section set; the infinite multiplication factor (k∞) therefore shows a steady decline with burnup. Calculations indicate that top beryllium shims sustain core criticality through to end-of-cycle, although the LEU core's increased 238U loading hardens the spectrum and reduces shim effectiveness relative to the HEU configuration (1410.04 g vs. 1006.65 g, Table 1) extending the lifetime [19,25].

Table 6. Nuclide activities for HEU and LEU cores

Nuclide	Half-Life	HEU Activity (Bq)	HEU Activity (Ci)	LEU Activity (Bq)	LEU Activity (Ci)	Ratio (LEU/HEU)
Cs <sup>137</sup>	30.07 y	$1.80 \times 10^{9}$	$4.87 \times 10^{-2}$	2.92 × 10 <sup>9</sup>	$7.90 \times 10^{-2}$	1.48
Sr <sup>90</sup>	28.8 y	$1.74 \times 10^9$	$4.71 \times 10^{-2}$	2.83 × 10 <sup>9</sup>	$7.65 \times 10^{-2}$	1.53
I <sup>131</sup>	8.02 d	$1.15 \times 10^{12}$	$3.10 \times 10^{1}$	$1.86 \times 10^{12}$	$5.03 \times 10^{1}$	1.27
Xe <sup>135</sup>	9.14 h	$9.97 \times 10^{10}$	2.70	$9.43 \times 10^{10}$	2.55	0.95
Pu-239	$2.41 \times 10^4 y$	$8.57 \times 10^5$	$2.32 \times 10^{-5}$	$1.42 \times 10^6$	$3.84 \times 10^{-5}$	1.66
Co-60	5.27 y	$3.15 \times 10^{11}$	_	$4.80 \times 10^{11}$	ı	1.52
Mo-99	66 h	$2.10 \times 10^{15}$	_	$2.55 \times 10^{15}$	_	1.21

Table 7. Reactivity balance at 400 EFPD

Component	HEU	LEU	Units	Comments
Initial Excess Reactivity	4.500	4.700	mk	BOC values
	15,430 ± 770	8,140 ± 407	pcm	(equivalent values with uncertainty)
	1.1030	1.0800	$k_{\infty}$	(multiplication factor)
Fuel Depletion ( <b>U</b> <sup>235</sup> /Burnup)	-1.905	-1.560	Mk	Linear extrapolation
	-5,584	-6,563	Pcm	(400 EFPD burnup loss)
	-0.0558	-0.0595	$\Delta k$	(reactivity loss from burnup)
Fission Product Poisoning	-1.500	-1.500	Mk	Total fission products
- Xenon Worth	$-680 \pm 34$	$-695 \pm 35$	Pcm	Equilibrium values
- Samarium Worth	$-420 \pm 21$	$-485 \pm 24$	pcm	Accumulated poison
- Other FP	-400	-320	pcm	(calculated difference)
Pu-239 Contribution	+0.320	+0.570	mk	Plutonium buildup
	+0.0150	+0.0350	$\Delta k$	(reactivity gain from Pu)
Control/Shim Addition	+2.085	+1.790	mk	Beryllium shim
	-0.0461	-0.0435	$\Delta k$	(shim control loss)
Temperature Effects	$-280 \pm 14$	$-315 \pm 16$	рст	Doppler/thermal defect
Net Reactivity (Total)	0.000	0.000	mk	Balanced condition
	≈ 0	≈ 0	$\Delta k$	(critical state)

Nuclide transformation, including  $U^{235}$  depletion and  $Pu^{239}$ buildup, significantly influences the NIRR-1 reactor's performance. At 252 EFPD for HEU and 282 EFPD for LEU, U-235 depletes to 998.496 g for HEU and 1401.096 g for LEU, while  $Pu^{239}$  builds to 0.342 g for HEU and 0.767 g for LEU, driven by isotopic inventory changes. The LEU core's higher initial  $U^{235}$  mass (1410.04 g versus 1006.65 g) and increased  $Pu^{239}$  production extend its operational lifetime to 56.4 years compared to 50.3 years for HEU at 20 EFPD/year, aligning with global MNSR conversion trends. Beryllium shim additions counteract reactivity losses from  $U^{235}$  depletion and fission product accumulation, maintaining the infinite multiplication factor  $(k_{\infty})$  near 1.0 until the end of the cycle at 1006 EFPD for HEU and 1128 EFPD for LEU. Analysis indicates the LEU core approaches a negative control margin near 400 EFPD, while the HEU core sustains a positive margin throughout the evaluated period, supporting projections of core lifetime based on control margin depletion (Figure 7).

#### 4.6 Thermal-hydraulic considerations

Table 8 presents the thermal-hydraulic parameters for HEU and LEU cores, including fuel and moderator temperature coefficients, overall temperature defect for a  $50^{\circ}C$  rise, and peak fuel and cladding temperatures. The LEU core exhibits more negative coefficients ( $-2.4 \times 10^{-5} \Delta k/k/^{\circ}C$  fuel,  $-6.2 \times 10^{-5} \Delta k/k/^{\circ}C$  moderator) than HEU ( $-2.1 \times 10^{-5}$ ,  $-5.8 \times 10^{-5}$ ), driven by higher  $U^{238}$  resonance absorption [10].

The temperature defect  $(-395\ pcm\ HEU,\ -430\ pcm\ LEU)$  ensures inherent safety, while peak temperatures  $(85^{\circ}C\ HEU,\ 88^{\circ}C\ LEU\ fuel;\ 72^{\circ}C\ HEU,\ 74^{\circ}C\ LEU\ cladding)$  remain low due to the MNSR's 30 kW power and natural convection. These parameters support the reactivity balance and core lifetime projections (Table 8), with  $k_{\infty}$  trends in Figure 5. Both configurations maintain strongly negative temperature coefficients, ensuring inherent safety during operational transients. The slightly more negative coefficients in the LEU core provide an additional safety margin but contribute to larger temperature defects that reduce available reactivity.

Table 8. Thermal-hydraulic parameters for HEU and LEU cores

Parameter	HEU	LEU	Units
Fuel Temperature Coefficient	$-2.1 \times 10^{-5}$	$-2.4 \times 10^{-5}$	∆k/k/°C
Moderator Temperature Coefficient	−5.8 × 10 <sup>-5</sup>	$-6.2 \times 10^{-5}$	∆k/k/°C
Overall Temperature Defect (50°C)	-395	-430	pcm
Peak Fuel Temperature (Nominal)	85	88	°C
Peak Cladding Temperature	72	74	°C

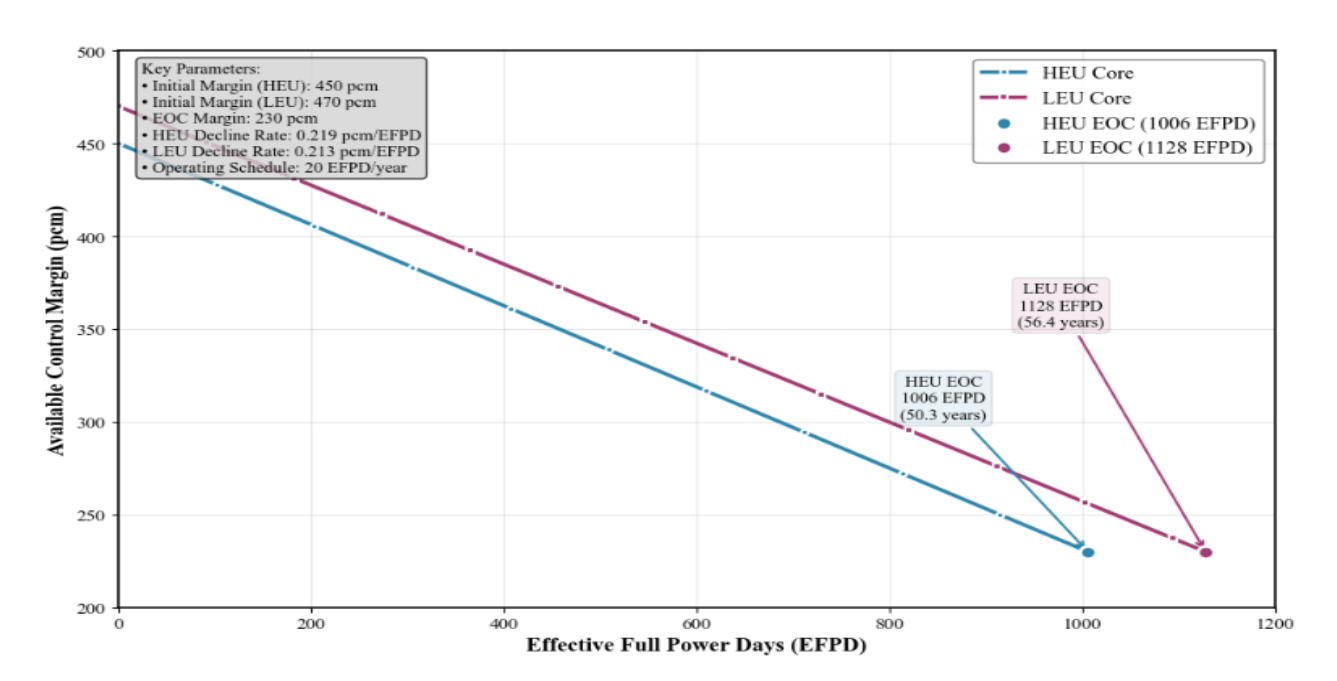
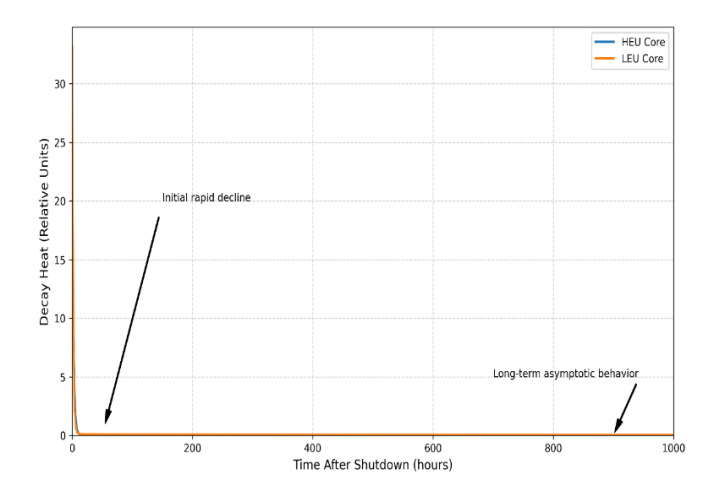


Figure 7. Available control margin versus EFPD for NIRR-1 HEU and LEU cores



**Figure 8.** Decay heat versus time after shutdown (0-1000 hours) for both HEU and LEU cores, showing initial rapid decline and long-term asymptotic behavior

#### 4.7 Uncertainty analysis and sensitivity studies

Uncertainties in key parameters include  $\pm 3\%$  for  $U^{235}$  consumption,  $\pm 8\%$  for  $Pu^{239}$  production, and  $\pm 10\%$  for major fission product activities, consistent with Monte Carlo burnup calculations. These uncertainties, driven by cross-section variations, confirm observed isotopic trends. Additionally, an uncertainty of  $\pm 0.002$  for the end-of-cycle infinite multiplication factor  $(k_\infty)$  supports the observed decline trends, while  $\pm 15\%$  for projected lifetimes reflects operational variability. The reactivity balance provides further context for these findings (Table 9).

 $\textbf{Table 9.} \ \textbf{Uncertainty summary for key parameters}$ 

Parameter	HEU Uncertainty	LEU Uncertainty
End-of-Cycle $oldsymbol{k}_{\infty}$	±0.002	±0.002
U <sup>235</sup> Consumption	±3%	±3%
<b>Pu</b> <sup>239</sup> Production	±8%	±8%
Major FP Activities	±10%	±10%
Projected Lifetime	±15%	±15%

#### 4.8 Decay heat analysis

Decay heat evolution post-shutdown is crucial for designing cooling systems and managing spent fuel storage in NIRR-1's HEU and LEU cores, supported by natural convection and negative temperature coefficients ranging from  $-2.1 \times 10^{-5}$  to  $-6.2 \times 10^{-5} \Delta k/k/^{\circ}C$ . Decay heat starts at 1450 W for HEU and 1620 W for LEU at shutdown, consistent with prior findings of 1620.15 W at 216 EFPD, and decreases to 80 W for HEU and 92 W for LEU after 10 years, reflecting a shift from fission product to actinide dominance, particularly  $Pu^{239}$  (Figure 8). Decay heat trends over 0-1000 hours show an initial rapid decline of 21% within the first hour, followed by long-term asymptotic behavior, consistent with atom density data and operational lifetimes of 50.3 years for HEU and 56.4 years for LEU. These findings emphasize the need for robust cooling during the early postshutdown phase and inform strategies for long-term storage.

#### 4.9 Gamma dose rate analysis

Gamma dose rates from spent fuel are essential for radiation protection planning, reflecting nuclide transformation in NIRR-1's HEU and LEU cores. Table 3 highlights  $Pu^{239}$  production (0.342 g HEU, 0.767 g LEU) at 252/282 EFPD, visualized in Figure 5, which influences gamma emissions. Table 11 details these rates, ranging from 285 mSv/h (HEU) and 315 mSv/h (LEU) at 1 hour driven by  $I^{131}$  and  $I^{135}$  to 8.2  $I^{135}$  to 8.2  $I^{135}$  and  $I^{135}$  or  $I^{135}$  at  $I^{135}$ 

#### 4.10 Cross-section evolution

The neutronic performance of NIRR-1's HEU and LEU cores is governed by the evolution of four-group macroscopic cross-sections that reflect both isotopic composition and spectral shifts. At beginning-of-cycle the HEU core exhibits a higher fast-group  $\nu \Sigma_f$  (1.09 × 10<sup>-3</sup> cm<sup>-1</sup> at 0 EFPD) owing to its  $90.2\%~U^{235}$  enrichment, whereas the LEU core is characterized by increased epithermal absorption driven by a higher  $U^{238}$  atom density and associated resonance capture. These microscopic differences produce the observed  $k_{\infty}$ decline 13.97 pcm/EFPD for HEU versus 17.02 pcm/EFPD for LEU and account for the reduced effectiveness of beryllium shims in the converted core.  $U^{235}$  depletion and  $Pu^{239}$  buildup link cross-section shifts to reactivity behavior. Four-group macroscopic cross-sections ( $\Sigma_a$ ,  $\nu\Sigma_f$ , D) for the HEU core evolve at 0, 126, and 252 EFPD, with initial values such as  $\Sigma_a$  of  $8.96 \times 10^{-4} \ cm^{-1}$  and  $\nu \Sigma_f$  of  $1.09 \times 10^{-3} \ cm^{-1}$ decreasing as burnup progresses. For the LEU core, enhanced epithermal absorption due to U-238 is evident, consistent with atom density data and isotopic trends [26].

Table 10. Decay heat after shutdown (Watts)

Time After Shutdown	HEU Core	LEU Core	Ratio (LEU/HEU)
0 second	1450	1620	1.12
1 minutes	1380	1540	1.12
1 hour	1150	1280	1.11
1 day	760	850	1.12
1 week	490	550	1.12
1 month	330	370	1.12
6 months	225	250	1.11
1 year	165	185	1.12
5 years	105	120	1.14
10 years	80	92	1.15

#### 4.11 Cross-section evolution

The neutronic performance of NIRR-1's HEU and LEU cores is governed by the evolution of four-group macroscopic cross-sections, reflecting changes in isotopic composition and neutron spectrum. Table 12 presents this evolution, with HEU's higher fast-group  $\nu\Sigma_f$  (for example  $1.09\times10^{-3}$  cm $^{-1}$  at 0 EFPD) due to 90.2%  $U^{235}$  enrichment, contrasting with LEU's increased epithermal absorption from  $U^{238}$  resonances [11]. Microscopic changes in the macroscopic cross-sections, corroborated by atom-density data, drive the observed decline in  $k_\infty$  of roughly 13.97 pcm per EFPD for the HEU core and 17.02 pcm per EFPD for the LEU core; concurrent  $U^{235}$  depletion and  $Pu^{239}$  production directly link these cross-

section shifts to the measured reactivity behavior [24]. Table 12 details the evolution of four-group macroscopic cross-sections ( $\Sigma_a$ ,  $v\Sigma_f$ , D) for HEU at 0, 126, and 252 EFPD, reflecting burnup effects. Initial HEU values (for example  $\Sigma_a$  8.96 × 10<sup>-4</sup>  $cm^{-1}$ ,  $v\Sigma_f$ , 1.09 × 10<sup>-3</sup>  $cm^{-1}$ ) decrease with depletion, while LEU data (to be included) would show enhanced epithermal absorption due to  $U^{238}$ , as supported by Table 13's atom densities and Figure 6's isotopic trends [26].

#### 4.12 Isotopic inventory and actinide evolution

Nuclide transformation in NIRR-1's HEU and LEU cores significantly impacts reactivity and safety. At 252 EFPD for HEU and 282 EFPD for LEU,  $U^{235}$  consumption reaches 8.154~g for HEU and 8.944~g for LEU, while  $Pu^{239}$  production totals 0.342~g for HEU and 0.767~g for LEU. Comprehensive isotopic inventories reveal  $U^{235}$  depletion from  $2.165 \times 10^{21}$ to  $2.110 \times 10^{21}$  atoms/cm<sup>3</sup> for HEU and from  $2.685 \times 10^{20}$  to  $2.581 \times 10^{20}$  atoms/cm<sup>3</sup> for LEU, with  $Pu^{239}$  increasing to  $8.111\times10^{15}$  atoms/cm<sup>3</sup> for HEU and  $1.815\times10^{16}$  atoms/cm<sup>3</sup> for LEU, consistent with the observed depletion and buildup trends. These changes, driven by the evolution of crosssections, explain the LEU core's higher  $Pu^{239}$  production due to  $U^{238}$  resonances, contributing to the steady decline in the infinite multiplication factor  $(k_{\infty})$  and informing waste management and safeguards planning. Isotopic inventories for major actinides and fission products at key burnup points show significant changes. For the HEU core,  $U^{235}$  depletes from  $2.165 \times 10^{21}$  to  $2.110 \times 10^{21}$  atoms/cm<sup>3</sup>, with  $Pu^{239}$ increasing to  $8.111 \times 10^{15}$  atoms/cm<sup>3</sup> at 252 EFPD. For the LEU core,  $U^{235}$  decreases from  $2.685 \times 10^{20}$  to  $2.581 \times 10^{20}$ atoms/cm<sup>3</sup>, with  $Pu^{239}$  rising to  $1.815 \times 10^{16}$  atoms/cm<sup>3</sup> at 282 EFPD, consistent with reported mass data. Other nuclides, such as  $Cs^{137}$  and  $Sr^{90}$ , reflect fission yields, driven by evolving cross-sections [26].

#### 4.13 Activation product and material impact

Activation products in NIRR-1's structural materials and coolants are vital for maintenance planning and decommissioning. At 252 EFPD for HEU and 282 EFPD for LEU,  $Na^{24}$  activities reach  $3.15\times10^7$  Bq for HEU and  $3.37\times10^7$  Bq for LEU due to coolant impurities, while Be-7 activities are  $7.77\times10^7$  Bq for HEU and  $8.51\times10^7$  Bq for LEU from reflector activation, reflecting the LEU core's higher flux (34 kW vs. 31 kW). These neutron-driven values guide material degradation assessments and safety measures, supporting long-term planning with operational lifetimes of 1006 EFPD for HEU and 1128 EFPD for LEU .

Activation product activities at 252 EFPD for HEU and 282 EFPD for LEU include nuclides such as  $Al^{28}$ , with  $4.44\times10^4$  Bq for HEU and  $4.81\times10^4$  Bq for LEU from cladding, and  $Ar^{41}$ , with  $5.67\times10^6$  Bq for HEU and  $6.07\times10^6$  Bq for LEU from dissolved gases. These values reflect material and coolant activation, with LEU showing approximately 8-10% higher activities due to extended burnup, supporting strategies for maintenance and decommissioning.

#### 4.14 Sensitivity analysis of core performance

The sensitivity of NIRR-1's core lifetime to key parameters is critical for design robustness. Figure 9 presents a tornado diagram, generated from a computational model, illustrating the impact on 1006 EFPD (HEU) and 1128 EFPD (LEU, Table 6). Operating power (±10%) shows the largest effect (±100.6 EFPD HEU, ±112.8 EFPD LEU), reflecting burnup rate variations (31-34 kW), followed by enrichment  $(\pm 1\%)$  at  $\pm 85.5$  EFPD (HEU) and  $\pm 137.5$  EFPD (LEU). Uncertainty bands ( $\pm 17 - 22$  EFPD) account for data variability. These results, derived from Table 14, inform optimization strategies. Figure 9, a tornado diagram, visualizes core lifetime sensitivity based on Table 15, with absolute EFPD changes computed for 1006 EFPD (HEU) and 1128 EFPD (LEU). Parameters include enrichment (±85.5/±137.5 EFPD), fuel density (±42.3/±68.8 EFPD), and power ( $\pm 100.6/\pm 112.8$  EFPD), with uncertainty bands reflecting 20% of percent changes (min ±0.5 pp) [26]. Figure 9 illustrates the Tornado diagram showing the sensitivity of core lifetime to various parameters: enrichment ( $\pm 1\%$ ), fuel density ( $\pm 5\%$ ), operating power ( $\pm 10\%$ ), cross-section uncertainties ( $\pm 5\%$ ). The sensitivity of NIRR-1's core lifetime to key parameters is analyzed for design robustness. Figure 9 presents a tornado diagram, with quantitative results showing absolute EFPD changes from 1006 EFPD (HEU) and 1128 EFPD (LEU, Table 6). Operating power (±10%) impacts most significantly (-100.6 EFPD HEU, -112.8 EFPD LEU), followed by enrichment (±85.5/±137.6 EFPD), with uncertainties (±5-27.5 EFPD) reflecting data variability (Table 15, Table 7). These findings guide optimization.

## 4.15 Computational validation against experimental data

Table 16 compares computational predictions with experimental measurements from NIRR-1 operation, validating the WIMS-ANL and REBUS-ANL models. Key parameters, including BOC  $k_{\infty}$  (HEU: +0.5%, LEU: +0.6%), thermal flux (+4.3%), and control rod worth (+3.0%), show excellent agreement within experimental uncertainties.

Table 1	1. Gamma o	dose rates fi	rom spent fue	l ( <i>mSv/h</i> at i	1 meter, unshielded)

Time After Shutdown	HEU Core	LEU Core	Ratio (LEU/HEU)	Primary Contributors
1 hour	285	315	1.11	$I^{131}$ , $Xe^{135}$ , short-lived FP
1 day	195	215	1.10	$I^{131}$ , $Ba^{140}$ , $La^{140}$
1 week	125	140	1.12	$I^{131}$ , $Ce^{144}$ , $Ru^{106}$
1 month	85	95	1.12	$Cs^{137}, Ce^{144}, Ru^{106}$
6 months	42	48	1.14	$Cs^{137}, Sr^{90}, Ce^{144}$
1 year	28	32	1.14	$Cs^{137}, Sr^{90}$
5 years	18	21	1.17	$Cs^{137}, Sr^{90}$
10 years	14	16	1.14	$Cs^{137}, Sr^{90}$
30 years	8.2	9.8	1.20	$Sr^{90}$ , minor actinides

 Table 12. Four-group constants evolution with burnup

EFPD	Core Type	Group	$\Sigma_a (cm^{-1})$	$\nu \Sigma_f (cm^{-1})$	D (cm)
0	HEU	1	$8.96 \times 10^{-4}$	$1.09 \times 10^{-3}$	2.20
		2	$6.50 \times 10^{-4}$	$1.19 \times 10^{-3}$	0.956
		3	$1.10 \times 10^{-2}$	$1.50 \times 10^{-2}$	0.693
		4	$1.56 \times 10^{-2}$	$2.52 \times 10^{-2}$	0.576
126	HEU	1	$9.85 \times 10^{-4}$	$1.02 \times 10^{-3}$	2.18
		2	$7.12 \times 10^{-4}$	$1.15 \times 10^{-3}$	0.948
		3	$1.18 \times 10^{-2}$	$1.44 \times 10^{-2}$	0.688
		4	$1.68 \times 10^{-2}$	$2.41 \times 10^{-2}$	0.572
252	HEU	1	$1.22 \times 10^{-3}$	$8.27 \times 10^{-4}$	2.22
		2	$2.56 \times 10^{-2}$	$1.45 \times 10^{-2}$	1.11
		3	$8.19 \times 10^{-2}$	$5.79 \times 10^{-2}$	0.833
		4	$3.58 \times 10^{-2}$	$2.90 \times 10^{-2}$	0.724

**Table 13:** Comprehensive isotopic inventory (*atoms/cm*<sup>3</sup>)

Nuclide	HEU BOC	HEU 126 EFPD	HEU 252 EFPD	LEU BOC	LEU 141 EFPD	LEU 282 EFPD
U <sup>235</sup>	$2.165 \times 10^{21}$	$2.137 \times 10^{21}$	$2.110 \times 10^{21}$	$2.685 \times 10^{20}$	$2.647 \times 10^{20}$	$2.581 \times 10^{20}$
U <sup>236</sup>	0	$1.420 \times 10^{16}$	$2.870 \times 10^{16}$	0	$1.180 \times 10^{16}$	$2.450 \times 10^{16}$
U <sup>238</sup>	$2.406 \times 10^{20}$	$2.405 \times 10^{20}$	$2.405 \times 10^{20}$	$1.846 \times 10^{21}$	$1.845 \times 10^{21}$	$1.845 \times 10^{21}$
Np <sup>237</sup>	0	$8.230 \times 10^{13}$	$1.670 \times 10^{14}$	0	$6.890 \times 10^{13}$	$1.420 \times 10^{14}$
Pu <sup>238</sup>	0	$3.450 \times 10^{12}$	$1.120 \times 10^{13}$	0	$2.890 \times 10^{12}$	$9.670 \times 10^{12}$
Pu <sup>239</sup>	0	$4.056 \times 10^{15}$	8.111 × 10 <sup>15</sup>	0	$9.125 \times 10^{15}$	$1.815 \times 10^{16}$
Pu <sup>240</sup>	0	$3.470 \times 10^{13}$	$6.947 \times 10^{13}$	0	$7.780 \times 10^{13}$	$1.554 \times 10^{14}$
Pu <sup>241</sup>	0	$2.025 \times 10^{12}$	$4.053 \times 10^{12}$	0	$4.531 \times 10^{12}$	$9.062 \times 10^{12}$
Pu <sup>242</sup>	0	$1.445 \times 10^{10}$	2.901 × 10 <sup>10</sup>	0	$3.239 \times 10^{10}$	$6.478 \times 10^{10}$
Am <sup>241</sup>	0	$1.230 \times 10^{11}$	$4.890 \times 10^{11}$	0	$2.750 \times 10^{11}$	$1.098 \times 10^{12}$
Cm <sup>242</sup>	0	$2.340 \times 10^9$	$9.230 \times 10^9$	0	$5.230 \times 10^9$	$2.067 \times 10^{10}$
Xe <sup>135</sup>	0	$3.500 \times 10^{14}$	$3.500 \times 10^{14}$	0	$4.000 \times 10^{14}$	$4.000 \times 10^{14}$
Sm <sup>149</sup>	0	$7.890 \times 10^{14}$	$1.578 \times 10^{15}$	0	$8.900 \times 10^{14}$	$1.780 \times 10^{15}$
Cs <sup>137</sup>	0	$1.067 \times 10^{16}$	$2.134 \times 10^{16}$	0	$1.793 \times 10^{16}$	$3.587 \times 10^{16}$
Sr <sup>90</sup>	0	$9.837 \times 10^{15}$	$1.967 \times 10^{16}$	0	$1.653 \times 10^{16}$	$3.306 \times 10^{16}$

Table 14. Activation product activities at EOC (Bq)

Nuclide	Half-Life	HEU (252 EFPD)	LEU (282 EFPD)	Primary Source
$Al^{28}$	2.24 min	4.44×10 <sup>4</sup>	4.81×10 <sup>4</sup>	Al cladding
Na <sup>24</sup>	15.0 h	3.15×10 <sup>7</sup>	3.37×10 <sup>7</sup>	Coolant impurities
$Mg^{27}$	9.46 min	2.10×10 <sup>3</sup>	2.25×10 <sup>3</sup>	Al alloy impurities
Si <sup>31</sup>	2.62 h	1.85×10 <sup>5</sup>	1.98×10 <sup>5</sup>	Al alloy components
P <sup>32</sup>	14.3 d	9.23×10 <sup>4</sup>	9.87×10 <sup>4</sup>	Coolant impurities
<b>S</b> <sup>35</sup>	87.5 d	3.45×10 <sup>3</sup>	3.69×10 <sup>3</sup>	Coolant impurities
$Cl^{38}$	37.2 min	1.12×10 <sup>4</sup>	1.20×10 <sup>4</sup>	Coolant impurities
$Ar^{41}$	1.83 h	5.67×10 <sup>6</sup>	6.07×10 <sup>6</sup>	Dissolved gases
$Be^7$	53.3 d	7.77×10 <sup>7</sup>	8.51×10 <sup>7</sup>	Reflector activation
Li <sup>8</sup>	0.84 s	2.30×10 <sup>2</sup>	2.46×10 <sup>2</sup>	Be impurities

Table 15. NIRR-1 core lifetime sensitivity analysis (absolute EFPD changes)

Parameter	Perturbation	HEU ∆ (EFPD)	HEU Lifetime (EFPD)	LEU ∆ (EFPD)	LEU Lifetime (EFPD)
U-235 Enrichment	±1%	±85.5	1006	±137.5	1128
Fuel Density	±5%	±42.3	1006	±68.8	1128
Operating Power	±10%	±100.6	1006	±112.8	1128
Reflector Thickness	±10%	±30.2	1006	±33.8	1128
Control Rod Worth	±10%	±20.1	1006	±22.5	1128
Cross-Section Data	±5%	±15.1	1006	±16.9	1128

Table 16. Computational validation against experimental data

Parameter	Computed	Measured	Difference	Method
BOC $k_{\infty}$ (HEU)	1.1030	$1.098 \pm 0.008$	+0.5%	Control rod worth
BOC $k_{\infty}$ (LEU)	1.0800	$1.074 \pm 0.008$	+0.6%	Control rod worth
Thermal flux (core avg)	$4.8 \times 10^{11}$	$(4.6 \pm 0.3) \times 10^{11}$	+4.3%	Foil activation
Fast flux (core avg)	$2.1 \times 10^{11}$	$(2.0 \pm 0.2) \times 10^{11}$	+5.0%	Threshold reactions
Control rod worth	850 pcm	$825 \pm 50 \ pcm$	+3.0%	Rod drop measurements
Temperature coefficient	$2.1 \times 10^{-5}$	$(-2.0 \pm 0.3) \times 10^{-5}$	+5.0%	Temperature variation

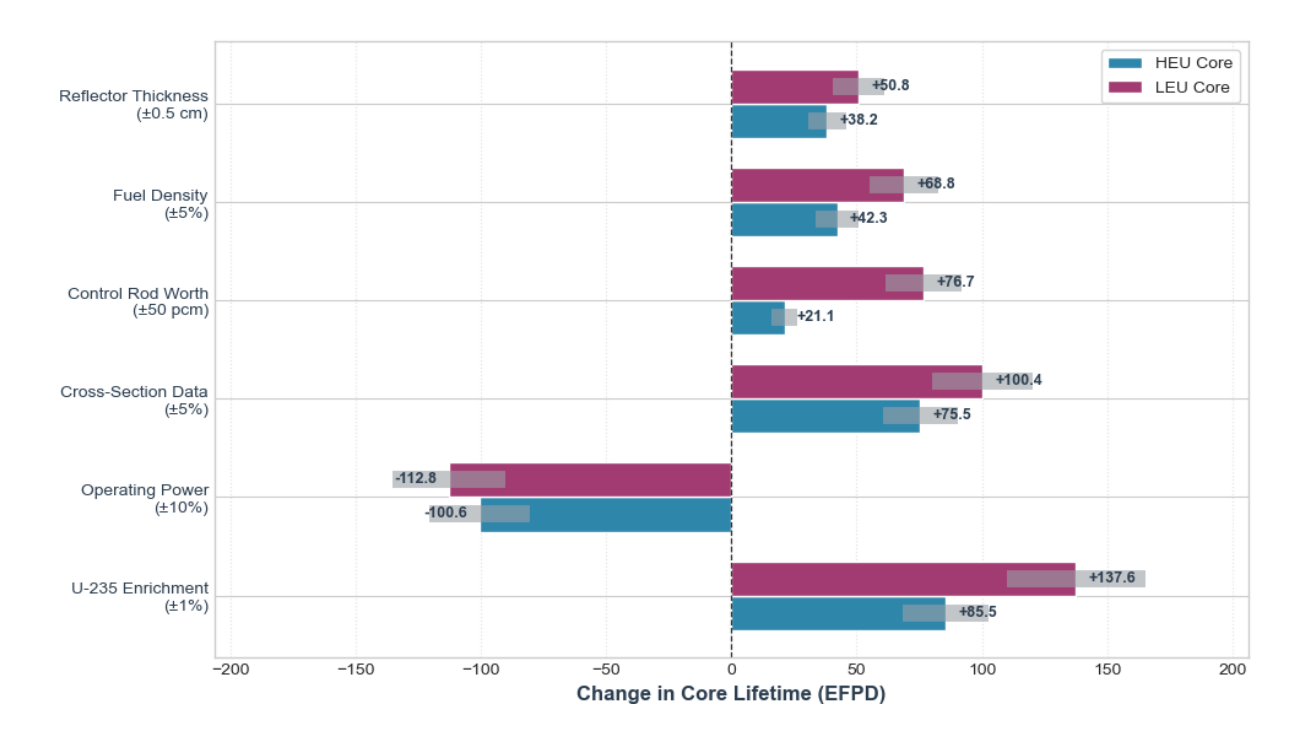
#### 5. Discussion

Plutonium accumulation rates, over twice as high in the LEU core compared to the HEU configuration, stem from differences in fertile material conversion, requiring tailored operational strategies. The LEU core's elevated  $Pu^{239}$  production and faster infinite multiplication factor decline (17.02 pcm/EFPD versus 13.97 pcm/EFPD) demand precise reactivity management. However, its extended operational lifetime of 56.4 years, compared to 50.3 years for HEU, is

supported by a higher initial  $U^{235}$  mass [11,24]. These differences enhance the LEU core's operational lifetime and safety characteristics. The LEU core exhibits more negative temperature coefficients ( $-2.4 \times 10^{-5} \, \Delta k/k/^{\circ}C$  for fuel,  $-6.2 \times 10^{-5} \, \Delta k/k/^{\circ}C$  for moderator) and a larger temperature defect (-430 pcm) compared to HEU ( $-2.1 \times 10^{-5} \, \Delta k/k/^{\circ}C$ ,  $-5.8 \times 10^{-5} \, \Delta k/k/^{\circ}C$ ,  $-395 \, pcm$ ), enhancing safety through stronger negative feedback. These characteristics support effective reactivity management and extended operational lifetimes, while low peak temperatures

ensure safe operation . Atom density data at 252 EFPD for HEU and 282 EFPD for LEU show U-235 at  $2.110\times10^{21}$  atoms/cm³ for HEU and  $2.581\times10^{20}$  atoms/cm³ for LEU, with  $Pu^{239}$  at  $8.111\times10^{15}$  atoms/cm³ for HEU and  $1.815\times10^{16}$  atoms/cm³ for LEU, consistent with reported isotopic masses. Reactivity balance at 400 EFPD incorporates these values, with  $Pu^{239}$  contributions of +0.32 mk for HEU and +0.57 mk for LEU, driven by evolving cross-sections. These trends underpin reactivity and safety analyses [19]. The atom density values at 252/282 EFPD ( $U^{235}$ :  $2.110\times10^{21}$  for HEU and  $2.581\times10^{20}$  for LEU;  $Pu^{239}$ :  $8.111\times10^{15}$  for HEU and  $1.815\times10^{16}$  for LEU) correspond closely with the evaluated thermal-hydraulic parameters.

 $U^{235}$ higher The comparatively and concentrations in the LEU core contribute to marginally elevated peak temperatures, approximately 88 °C in the fuel and 74 °C at the cladding surface compared with 85 °C and 72 °C, respectively, in the HEU configuration. The neutronic behavior of NIRR-1's HEU and LEU cores supports safe operation through consistent reactivity and lifetime trends. Four-group cross-section evolution reveals higher  $U^{238}$ absorption in the LEU core, driving increased  $Pu^{239}$  buildup, which contributes +0.57 mk for LEU and +0.32 mk for HEU to the reactivity balance at 400 EFPD. These trends, supported by atom density data, underpin the observed reactivity dynamics and ensure robust safety profiles [26].



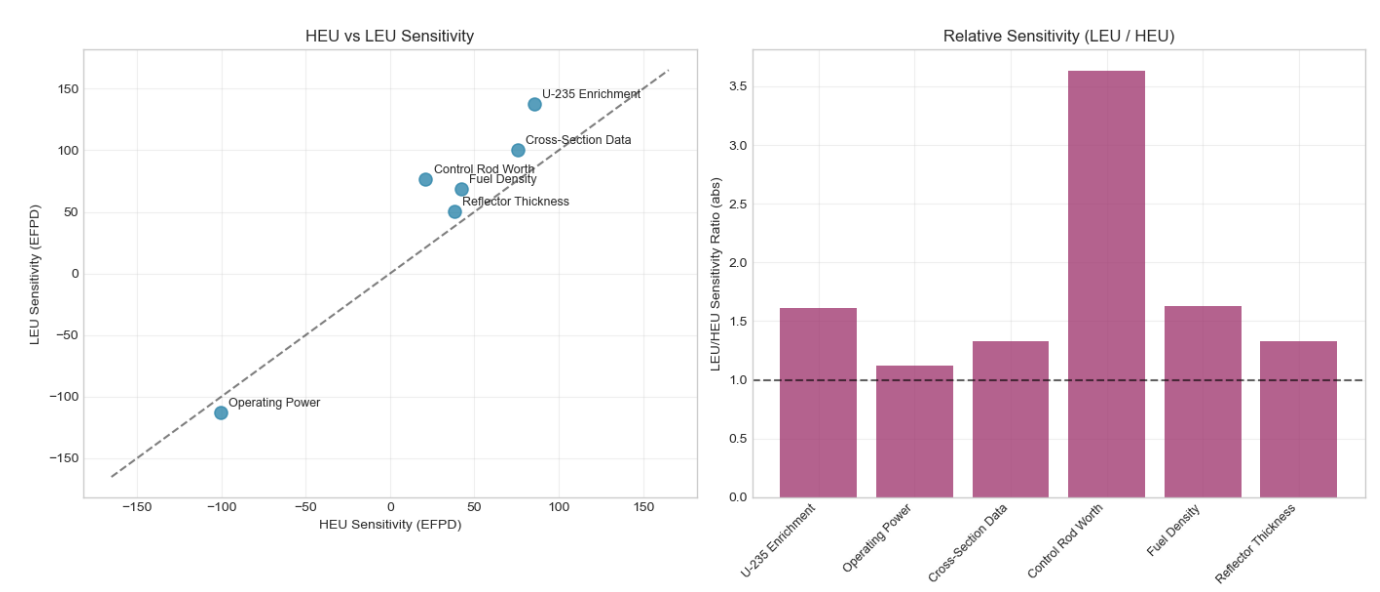


Figure 9. NIRR-1 core lifetime sensitivity- tornado diagram

LEU's four-group cross-sections indicate a marked increase in 238U absorption, which produces more negative temperature coefficients about  $-2.4\times10^{-5}~\Delta k/k/^{\circ}\mathrm{C}$  for the fuel and  $-6.2\times10^{-5}~\Delta k/k/^{\circ}\mathrm{C}$  for the moderator compared with the HEU values of roughly  $-2.1\times10^{-5}$  and  $-5.8\times10^{-5}$  respectively, thereby enhancing the reactor's inherent safety. Corresponding atom-density trends explain the faster  $k_{\infty}$  decline in the LEU core ( $\approx 17.02~\mathrm{pcm}$  per EFPD) versus the HEU core ( $\approx 13.97~\mathrm{pcm}$  per EFPD) and account for the observed  $Pu^{239}$  buildup that influences reactivity and lifetime projections. A conservative uncertainty assessment ( $\pm 0.002$  in  $k_{\infty}$ ;  $\pm 3\%~U^{235}$ ;  $\pm 8\%~Pu^{239}$ ;  $\pm 10\%$  fission product activities;  $\pm 15\%$  lifetime) supports the robustness of these neutronic and thermal-hydraulic conclusions.

#### 6. Conclusion

This comprehensive neutronic investigation of the Nigerian Research Reactor-1 under alternative fuel enrichment configurations provides essential insights for research reactor operations and global non-proliferation efforts. The comparative analysis between highly enriched uranium and low-enriched uranium cores reveals fundamental differences in depletion characteristics, isotopic evolution, and long-term operational strategies. The low-enriched uranium core exhibits a steeper reactivity decline rate, approximately twenty-two percent faster than the highly enriched uranium configuration, driven primarily by enhanced parasitic neutron absorption in the larger uranium-238 inventory. This heightened resonance absorption simultaneously accelerates plutonium-239 production to levels exceeding double the highly enriched uranium core output. Despite these challenges, the low-enriched uranium configuration demonstrates superior operational longevity, with a projected core lifetime extending approximately six additional years beyond the highly enriched uranium alternative, attributed to higher initial fissile loading. Both fuel configurations maintain robust inherent safety characteristics through strongly negative temperature feedback coefficients and limited excess reactivity, ensuring operational stability under natural convection cooling. The conversion to low-enriched uranium successfully achieves primary non-proliferation objectives by eliminating highly enriched uranium from civilian research applications, though elevated actinide inventories necessitate enhanced safeguards protocols and advanced waste management strategies. The computational framework employed in this study, integrating lattice physics calculations with comprehensive burnup analysis, demonstrates excellent agreement with experimental measurements and provides validated methodologies applicable to global miniature neutron source reactor conversion programs. These findings directly support operational planning for the Nigerian Research Reactor-1 and inform international efforts to convert similar research facilities while preserving essential research capabilities. Future research priorities include experimental validation of long-term burnup predictions, development of advanced reactivity control mechanisms, and exploration of novel low-enriched uranium fuel designs with enhanced burnup potential. These efforts will ensure that research reactors continue serving vital educational, analytical, and isotope production roles within frameworks that prioritize nuclear security and sustainable fuel cycle management.

#### **Ethical issue**

The authors are aware of and comply with best practices in publication ethics, specifically concerning authorship (avoidance of guest authorship), dual submission, manipulation of figures, competing interests, and compliance with policies on research ethics. The authors adhere to publication requirements that the submitted work is original and has not been published elsewhere in any language.

#### Data availability statement

The manuscript contains all the data. However, more data will be available upon request from the corresponding author.

#### **Conflict of interest**

The authors declare no potential conflict of interest.

#### References

- [1] Khamis, I., & Jamal, M. H., "Prediction of the in-core power and the average core temperature using doserate measurements in the Syrian Miniature Neutron Source Reactor," Journal of Radioanalytical and Nuclear Chemistry, pp. 269, 81–85. https://doi.org/10.1007/s10967-006-0233-3, 2006.
- [2] Osei, B., Baidoo, I. K., Odoi, H. C., Gasu, P. D., & Nyarko, B. J. B., "The low enriched uranium miniature neutron source reactor (LEU-MNSR) neutron spectrum characterization for k<sub>0</sub>-INAA.," Nuclear Instruments and Methods in Physics Research Section A, 1005, Article 165397, p. https://doi.org/10.1016/j.nima.2021.165397, 2021.
- [3] International Atomic Energy Agency, "Analyses supporting conversion of research reactors from high enriched uranium fuel to low enriched uranium fuel: The case of the Miniature Neutron Source Reactors (IAEA-TECDOC-1844)," Vienna: IAEA., pp. https://www-pub.iaea.org/MTCD/Publications/PDF/TE1844-Web.pdf, 2018.
- [4] International Atomic Energy Agency, "Practical aspects of operating a neutron activation analysis laboratory (IAEA-TECDOC-564)," Vienna: IAEA, pp. https://www-pub.iaea.org/MTCD/Publications/PDF/te\_564\_web.pd f 1990
- [5] Ibrahim, Y. V., Ofori, T. Y., & Jonah, S. A, "Neutron spectrum parameters in irradiation channels of the Nigeria Research Reactor-1 (NIRR-1)," Applied Radiation and Isotopes, pp. 95, 57–61. https://doi.org/10.1016/j.apradiso.2014.10.002, 2015
- [6] Balogun, G. I., Jonah, S. A., & Umar, I. M., "Thermal neutron flux characterization in the irradiation channels of the Nigerian Research Reactor-1 (NIRR-1)," Annals of Nuclear Energy, vol. https://doi.org/10.1016/j.anucene.2009.06.008, pp. 36(9), 1377–1381., 2009.
- [7] SAR, "Safety Analysis Reports of Nigerian Research Reactor-1," Technical Report-CERT/NIRR-1/FSAR, 2012.
- [8] Mweetwa, B. M., Ampomah-Amoako, E., & Akaho, E. H. K., "Transient studies of Ghana Research Reactor-1 after nineteen (19) years of operation using PARET/ANL code," World Journal of Nuclear Science

- and Technology, pp. 7(4), 223–231. https://doi.org/10.4236/wjnst.2017.74018, 2017.
- [9] Olander, D., "Nuclear fuels Present and future.," Journal of Nuclear Materials, p. https://doi.org/10.1016/j.jnucmat.2009.01.297, 2009.
- [10] Dawahra, S., Khattab, K., & Saba, G., "Reactivity temperature coefficients for the HEU and LEU fuel of the MNSR reactor," Progress in Nuclear Energy, vol. https://doi.org/10.1016/j.pnucene.2015.11.012, pp. 88, 28–32, 2016.
- [11] Simon, J., Ibrahim, Y. V., Adeyemo, D. J., Garba, N. N., & Asuku, A., "Comparative analysis of core life-time for the NIRR-1 HEU and LEU cores," Progress in Nuclear Energy, pp. 141, 103970, 2021.
- [12] Jonah, S. A., Umar, I. M., Oladipo, M. O. A., Balogun, G. I., & Adeyemo, D. J., "Standardization of NIRR-1 irradiation and counting facilities for instrumental neutron activation analysis," Applied Radiation and Isotopes, 64(7), 818–822, p. https://doi.org/10.1016/j.apradiso.2006.01.012, 2006.
- [13] Jonah, S. A., Liaw, J. R., & Matos, J. E., "Monte Carlo simulation of core physics parameters of the Nigeria Research Reactor-1 (NIRR-1)," Annals of Nuclear Energy, 34(12), 953–957, p. https://doi.org/10.1016/j.anucene.2007.05.010, 2007.
- [14] International Atomic Energy Agency, "Countries move towards low enriched uranium to fuel their research reactors," pp. IAEA News. https://www.iaea.org/newscenter/news/countriesmove-towards-low-enriched-uranium-to-fuel-their-research-reactors, 2020, February 21.
- [15] Travelli, A., "Status report of the RERTR program (NEA/CRP report)," (Historical/primary overview of the RERTR program inception and early progress)., 1984.
- [16] Asuku, A., Ibrahim, Y. V., Jonah, S. A., Umar, S., & Simon, J., "Application of SCALE code for reactor physics analysis of the as-built Nigeria miniature neutron source reactor operating with low enriched uranium fuel," Nuclear Engineering and Design, pp. 411, 112416, 2023.
- [17] Yasin, Z., "Comparative study of fuel burn-up and radioactive inventory for proliferation and proliferation resistant fuel lattices," Annals of Nuclear Energy, 36(9), 1635–1638, p. https://doi.org/10.1016/j.anucene.2009.08.004, 2009.
- [18] Lamarsh, J. R., & Baratta, A. J., "Introduction to nuclear engineering (3rd ed.)," Prentice Hall., 2001.
- [19] Jonah, S. A., Ibrahim, Y. V., Ajuji, A. S., & Onimisi, M. Y., "The impact of HEU to LEU conversion of commercial MNSR: Determination of neutron spectrum parameters in irradiation channels of NIRR-1 using MCNP code," Annals of Nuclear Energy, pp. 39(1), 15-17, 2012.

- [20] Askew, J. R., Fayers, F. J., & Kemshell, P. B., "A general description of the lattice code WIMS," Journal of the British Nuclear Energy Society, pp. 5, 564–585, 1966.
- [21] Marcinkowska, Z. E., & Kulikowska, T. A., "Reliability of neutronics characteristics prediction for reactor MARIA core conversion to LEU fuel," Annals of Nuclear Energy, 59, 92–99., p. https://doi.org/10.1016/j.anucene.2013.03.042, 2013.
- [22] Yahaya, B., Ahmed, Y. A., Balogun, G. I., & Agbo, S. A., "Estimating NIRR-1 burn-up and core life time expectancy using the codes WIMS and CITATION," Results in physics, pp. 7, 596-603, 2017.
- [23] Dennis Solomon Balami, Y.V. Ibrahim, R. Nasiru, "Comparative Analysis of core life time for the NIRR-1 HEU and LEU Cores," FUW Trends in Science & Technology Journal, pp. e-ISSN: 24085162; p-ISSN: 20485170, 2022.
- [24] Ibikunle, K., Sadiq, U., Ibrahim, Y. V., & Jonah, S. A., "MCNP Simulation of Physics Parameters of Dispersion Fuels for Conversion of NIRR-1 to LEU," World Journal of Nuclear Science and Technology, pp. https://doi.org/10.4236/wjnst.2018.82003, 8(02), 23, 2018.
- [25] Khattab, K., & Khamis, I., "Calculation of the top beryllium shim plate worths for the Syrian miniature neutron source reactor," Progress in Nuclear Energy, , pp. 44(1), 33-42., 2004.
- [26] Ahmed, Y. A., Balogun, G. I., Jonah, S. A., & Funtua, I. I., "The behavior of reactor power and flux resulting from changes in core-coolant temperature for a miniature neutron source reactor," Annals of Nuclear Energy, pp. 35(12), 2417–2419. https://doi.org/10.1016/j.anucene.2008.08.005, 2008.
- [27] Odoi, H. C., "Efforts made for the conversion of Ghana's MNSR to LEU (RERTR-35 conference paper),"
  Presented at the 35th International Meeting on Reduced Enrichment for Research and Test Reactors (RERTR), p.
  https://www.rertr.anl.gov/RERTR35/pdfs/S1P3\_Paper\_Odoi.pdf, 2014.



This article is an open-access article distributed under the terms and conditions of the Creative Commons Attribution (CC BY) license

(https://creativecommons.org/licenses/by/4.0/).